Novel Composites for Human Meniscus Replacement

Adijat Omowumi Inyang, Tamer Abdalrahman, and Christopher Leonard Vaughan

Keywords Meniscus · Composites · Fiber · Matrix · Mold · Meniscal prosthesis · Stainless steel · Wear · Tensile · Compression

1 Introduction

The menisci are an essential part in the knee, by settling the joint and distributing the force over the articulating surfaces [1, 2]. Consequently, the upkeep of the native menisci is indispensable for the proper functioning of the knee. The knee transmits significant forces of up to 3–5 times body weight, of which the meniscus is known to carry anywhere between 45 and 75% of such load [3–5]. This increases the contact area thereby shielding the underlying cartilage from experiencing high compressive stress [6, 7]. A meniscal replacement possessing similar biomechanical behavior therefore is expected to support recurrent stress from the femoral condyle during flexion-extension motions [8]. Furthermore, its load distribution capabilities are crucial so as to spread the load over a wide area such that the joint space is preserved. The mechanical performance of materials plays a major role in materials development. This is used for quality assessment and quality guarantee, to predict the material behavior under operating conditions different from those of the test and is also utilized in computations during design [9]. This is particularly relevant to composites designed for load-bearing applications.

One of the causes of the failure of meniscal devices is the incorrect choice of material used in their design [10]. This lack of required material properties eventually leads to breakage, wear and tear. A material that will serve as a replacement for the meniscus must be able to accommodate high stresses and hence the need to have

A. O. Inyang (✉) · C. L. Vaughan
Division of Biomedical Engineering, Department of Human Biology, Faculty of Health Sciences, University of Cape Town, Observatory, South Africa
e-mail: wumi.inyang@uct.ac.za; kit.vaughan@uct.ac.za

T. Abdalrahman
Mechanobiology Laboratory, Division of Biomedical Engineering, Department of Human Biology, Faculty of Health Sciences, University of Cape Town, Observatory, South Africa
e-mail: Tamer.abdalrahman@uct.ac.za

B. Li, T. Webster (eds.), *Orthopedic Biomaterials*,
https://doi.org/10.1007/978-3-319-73664-8_19

mechanical properties similar to that of the native meniscus. Messner et al. were the first to publish extensive articles on the capability of Teflon and Dacron biomaterials to fill in as lasting meniscal substitutes [11–13]. van Tienen et al. investigated the utilization of the permeable polyurethane scaffolds for meniscal substitutes. The porosity and compressive properties were adapted to empower tissue regeneration [14, 15]. Polyvinyl alcohol or PVA hydrogels have been used by American research groups for meniscal substitution. It has been presented that by combining the polyethylene filaments with the hydrogel both the tensile and compressive moduli of the biomaterial can be tuned to look like that of the local meniscus [16], which is an imperative stride towards the capacity of any meniscus embed to convert compressive load into circumferential stress. In addition, polyethylene reinforced polycarbonate-urethane (PCU) has been utilized as a meniscus implant [17–21].

In this work, we have fabricated composites of medical grade silicone elastomers reinforced with nylon fibers and PCU with Ultra High Molecular Weight Polyethylene (UHMWPE) fibers and nylon fibers for replacing the meniscus. The excellent mechanical properties, biocompatibility, and viscoelasticity of the matrices coupled with fiber's notable physical properties and durability makes the developed composites a potentially exceptional and desirable replacement for the meniscus.

2 Methods

2.1 Design of the Mold

A custom mold was designed for the production of the mechanical test samples. The mold was designed such that the reinforcing fibers can be pulled through the mold and arranged horizontally at equal intervals as well as being held in tension. A 3-dimensional geometric design was made using SolidWorks (Dassault Systèmes, Vélizy, France) CAD (computer aided design) software from which the casting of the mold was done. The mold was made in different parts so as to allow easy removal of the samples after curing. Figure 1 shows a cross section of the assembled mold. The design included an enclosure for the mold in order to contain and prevent the matrix from spilling out of the mold.

2.2 Composite Preparation

The composite materials were prepared using combinations of the different matrices and fibers:

1. Silicone elastomers and nylon fibers and
2. Polycarbonate-urethanes (PCU) with Ultra High Molecular Weight Polyethylene (UHMWPE) fibers and nylon fibers.

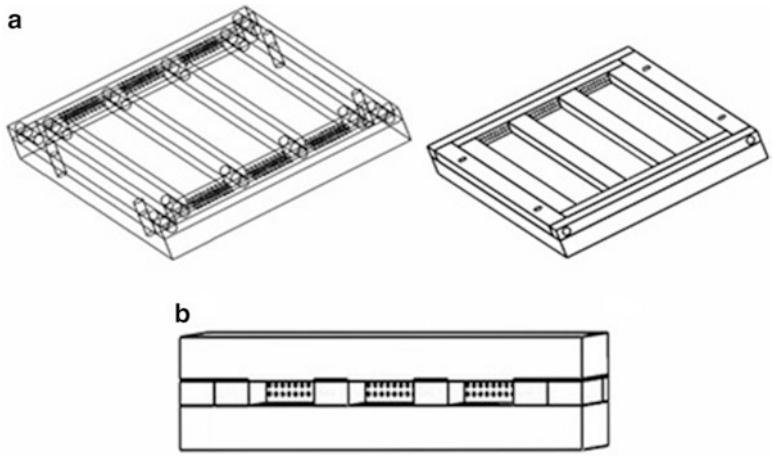

Fig. 1 (**a**) An assembly of the mold showing the screws and mold enclosure (**b**) Cross-sectional view of the mold for the mechanical test samples

Table 1 Typical properties of the different grades of silicone elastomers and the nylon fiber

Material property	Q7-4720	Q7-4765	Q7-4780	Nylon fiber	80A	90A	PE fiber
Durometer hardness	23	65	77	–			
Tear strength (kN/m)	32	45.1	41.7	–	64.9	96.4	
Tensile strength (MPa)	9	8	7.8	–	46.6	55.1	
Density (kg/m^3)	1110	1200	1200	1150	1190	1200	960
Elongation (%)	1310	900	660	–			
Elastic modulus (MPa)	–	–	–	3	12	29	
Breaking load (kg)	–	–	–	24.9			
Melting point (°C)	–	–	–	220			220

The medical grade silicones used were as follows: Silastic® biomedical grade enhanced tear resistant (ETR) silicone elastomers Q7-4720, Q7-4765 and Q7-4780 (Dow Corning Limited, Coventry, UK). Bionate PCU 80A and 90A pellets were supplied as spherical pellets by the DSM Polymer Technology Group (PTG, Berkeley, CA, USA) while the UHMWPE fibers (Dyneema Purity® UG) referred to as PE in this study were obtained from DSM. The properties of the matrices and fibers are shown in Table 1 as stated in the supplier's data sheets.

The fibers were manually pulled through the holes in the mold from one end to the other. Each fiber was held tightly in order to keep it in tension while the last fiber was dragged across a screw and tightened until the fibers were no longer slack. The fibers were arranged prior to the composite preparation as it was observed that leaving the fibers in the mold caused them to sag.

Having put in the fibers, the mold was filled with the mixed matrix and thereafter fixed into its enclosure. The rectangular cuboid (153 × 19 × 6 mm) samples (Fig. 2) were cured in a pre-heated hydraulic hot press (Moore E1127, Birmingham, UK) at

Fig. 2 Setup of the fiber arrangement in the mold (**a**) fiber aligned in the mold and (**b**) mold seated in its enclosure to retain the polymer

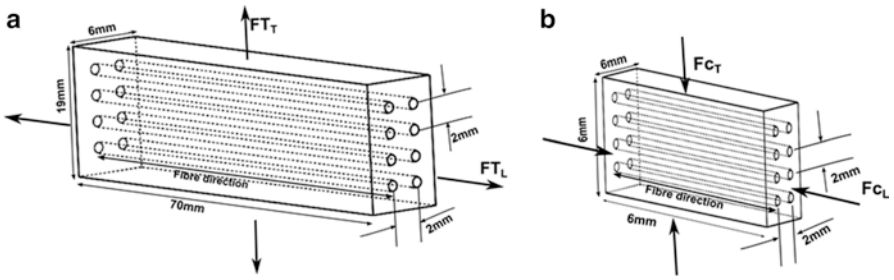

Fig. 3 Schematic view of the fabricated mechanical test piece showing the arrangement of the fibers and the direction of the tensile testing, Ft, along the fibers while the compression testing was carried out perpendicular to the fiber direction, Fc (L and T indicate to longitudinal and transverse)

116 °C for 3 h. The mold was allowed to cool for 24 h after which the samples were removed. The same process was followed for fabricating samples containing 100% polymeric matrix.

2.3 Mechanical Evaluation

Both tensile and compression testing were performed using a Zwick/Roell Z030 material testing machine (Leominster, Herefordshire, UK). Rectangular cuboid shaped (70 × 19 × 6 mm) specimens were cut and tested in tension, F_T (Fig. 3a). Each specimen was tested at a crosshead speed of 12 mm/min. Compression tests, Fc (Fig. 3b), were carried out with cubic (6 × 6 × 6 mm) specimens at a crosshead speed of 5 mm/min. Four specimens were used in each of the tests. All the results were computed as mean ± standard deviation and with Excel software (Microsoft, Washington, USA).

Fig. 4 The fabricated bench-top injection molding apparatus

2.4 Microstructural Analysis

With the aid of a Wild M400 (USA) light microscope the distribution and alignment of the fibers in the composites were observed, while a FEI XL-30 FEG model environmental scanning electron microscope (ESEM) was used to further establish the fiber alignment in the composite.

2.5 Meniscal Prosthesis Production

2.5.1 Injection Molding Machine

The production of the meniscal implants was done using an injection molding technique. A mini custom-built injection molding machine was designed and fabricated locally (Fig. 4). It includes two molds, one for fabricating the fiber-part and the other to produce the prosthesis. Each mold consisted of two separable parts for easy removal of molded parts.

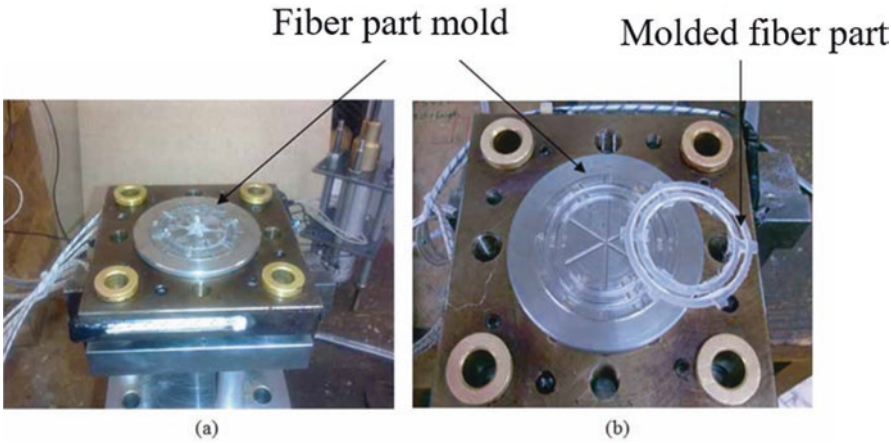

Fig. 5 The mold for fabricating the fiber-part (**a**) the molded fiber-part within the mold (**b**) the fiber-part after being removed from the mold

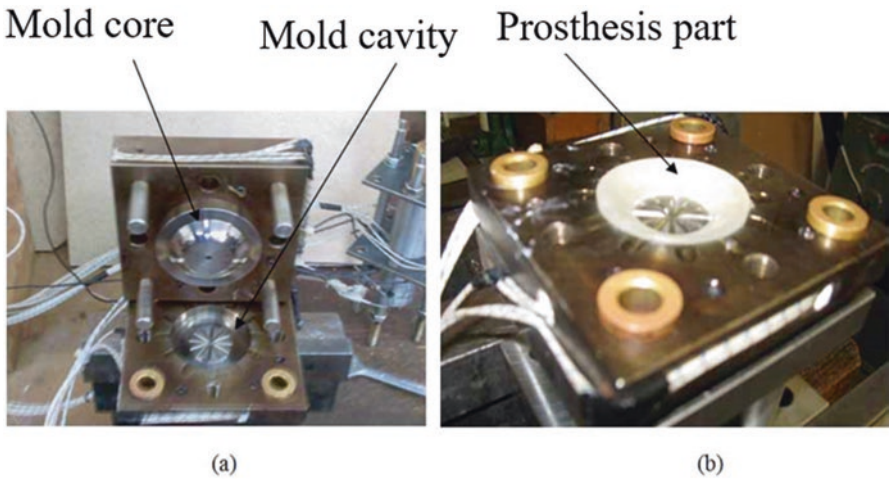

Fig. 6 The mold for fabricating the complete meniscal prosthesis (**a**) the mold core and cavity (**b**) the complete meniscal prosthesis within its mold

2.5.2 Meniscal Prosthesis Fabrication

Injection molding of the meniscal component was carried out in two stages. The fiber-part was first produced as a molded piece (Fig. 5) followed by an overmolding process [22]. This involved placing the molded fiber-part into the other mold and allowing molten matrix to fully cover the mold to produce a complete meniscal component (Fig. 6). In addition, the PCUs were molded without fibers to serve as controls.

Table 2 Composition of the different meniscal composites

Matrix	Fiber	Specimen type
Bionate 80A	–	B8
	Nylon	B8N
	PE	B8PE
Bionate 90A	–	B9
	Nylon	B9N
	PE	B9PE

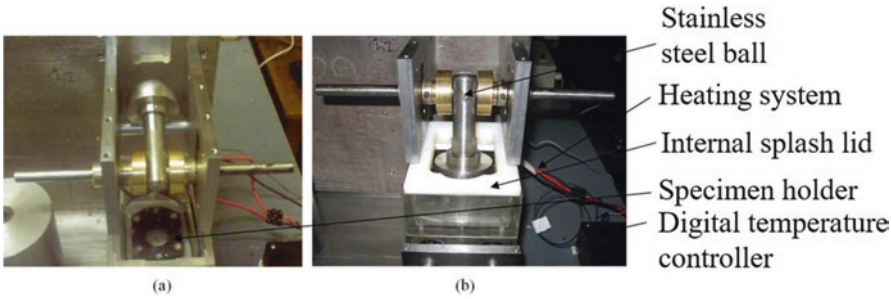

Fig. 7 The testing compartment for the friction and wear testing showing (**a**) the prosthesis holder fixed within the lubricant bath and (**b**) the stainless steel counterface seated on top of the specimen in its holder with the in-built heating system

Prior to processing, the PCU pellets were dried in a vacuum oven at 100 °C for 14 h, being the best drying conditions [23] and as recommended by the manufacturer to reduce its moisture content to approximately 0.01%. The materials composition for meniscus production are summarized in Table 2.

2.6 Friction and Wear Tests of Meniscal Prosthesis

2.6.1 Experimental Technique

A standard linear reciprocating wear rig used for testing the friction and wear behavior of the mensical prostheses was designed and built at the mechanical engineering department of the University of Cape Town [24, 25]. It is a customized wear rig that has been extensively used for testing the friction and wear properties of different materials [26]. The rig was designed to reproduce the sliding wear behavior of two materials moving against each other under different operating conditions. It consists of a flat counterface, fixed unto a shuttle base, which slides perpendicularly on a stationary wear pin. It operates in a reciprocating mode to test the required samples. In order to adapt this device as a simulated knee wear tester, new fixtures were designed and fabricated. Figure 7 shows a setup of the assembled fixtures.

The in vitro wear tests used were in accordance with the ASTM F732 standard, Standard Test Method for Wear Testing of Polymeric Materials Used in Total Joint Prostheses. This has been previously used to study hydrogels for articular cartilage replacement [27]. In this study, three prostheses were tested for each of the specimen types; they were thoroughly cleaned following the series of processes specified in the standard. These involved (a) rinsing the samples with tap water in order to eliminate bulk contaminants, (b) washing in an ultrasonic cleaner in a solution of 1% decon cleaning detergent for 15 min, (c) rinsing in a stream of distilled water, (d) washing in the ultrasonic cleaner in distilled water for 5 min, (e) rinsing again in a stream of distilled water, (f) drying with lint-free tissue, (g) immersing in methyl alcohol for 3 min, (h) drying with lint-free tissue, and finally (i) air-drying in dirt-free surroundings at room temperature for 30 min.

Each prosthesis specimen was weighed three times before the test to obtain an initial mass using a Mettler Toledo AT20 balance (Microsep (Pty) Ltd., Switzerland), having a sensitivity of 0.001 mg. The averages and standard deviations of these masses were calculated and used. Similarly, the means and standard deviations of the mass measurements of the specimens after the tests were computed. The lubricant used was bovine serum with a composition of 25% foetal calf serum (Highveld Biological (Pty) Ltd., South Africa) in 75% distilled water with the addition of 0.2% sodium azide to act as an antibiotic. The mixture was filtered using 0.22 μm filter to remove impurities; it was thereafter placed in sterilized bottles and kept frozen at −20 C until use.

The tests utilized a stainless steel counterface under a limited normal load of 360 N, being the maximum the machine could tolerate without exceeding the capacity of the motor. Also, beyond this load limit, the wear rig makes excessive noise. Besides, overloading the rig will compromise the test configuration. A collection of specimens was used as controls, loaded soak controls and unloaded soak controls to cater for each of the specimen types. These controls were used to estimate the difference in fluid uptake between the tested specimens and the control specimens during the gravimetric wear calculations. In addition, effort was made to verify the precise wear of the tested specimens by drying them in the vacuum oven before and after the test to completely remove the absorbed lubricant during the test. The drying was done in the vacuum oven at 50°C while checking the weight periodically until a stable weight was obtained to ascertain complete removal of fluid. Mass loss was measured using a microbalance, each mass being measured three times and their averages recorded.

2.6.2 Description of the Test

The specimen was first secured into the specimen holder affixed to the lubricant bath. The bath was then mounted onto a mechanism which consisted of a shuttle base that housed linear bearings, this mechanism was attached via a connecting shaft to a friction measuring load cell linked to a crank shaft driven by an electric motor. The lubricant of approximately 210 mL was poured into the testing chamber,

which was up to three quarters of its volume, allowing the contact surfaces to be well immersed in the test medium. The stainless steel counterface was placed into the chamber to sit on the specimen, positioning the convex surface of the counterface to fit precisely into the inner curvature of the specimen. On starting the motor, it drove the mechanism which in turn made the stainless steel counterface to swing such that it was subjected to a simple harmonic oscillatory motion with a stroke of ±15° in flexion/extension simulating a walking cycle. The movement of the counterface was aided by the attached weight bearing shaft and bushes; at a frequency of 1 Hz and a speed of 60 mm/s in a linear reciprocating motion of 30 mm length making a full cycle 60 mm. Although sliding speed had been estimated to be 50 mm/s and 150 mm/s for walking and running in the human knee [28], the oscillating speed of 60 mm/s was chosen, being the minimum permitted by the adjustable screw of the specialized wear equipment. Each test was carried out for a total number of 100,000 cycles while maintaining the temperature of the test fluid at a physiological temperature of 37 ± 1±°C. The total number of 100,000 cycles is another limitation which is because the rig could not be allowed to run consecutively for several days due to the capacity of its motor.

The frictional forces between the stainless steel counterface and the prosthesis specimen were measured using a calibrated load cell. The load cell, linked to the shuttle by a shaft, reads the forces as voltage values, amplifies and converts them to frictional data. A computer software application was used to obtain the data through a National Instruments data acquisition device. The frictional force data were written to a comma-separated values (CSV) file. The conversion of the voltage (mV) / sample data to force (N)/distance (m) by the software uses the sample rate, reciprocating speed and load cell calibration.

2.6.3 Friction Measurements

The process of sampling for frictional force did not correspond to the movement of the test specimen. Therefore, while the cycle had a frequency of 1 Hz, sampling had a higher frequency of approximately 2.53 samples per second (2.53 Hz), the latter being previously fixed by the data acquisition software.

The friction coefficient, μ, was calculated using the frictional force, F_F, and the normal load, F_N as in Eq. (1).

$$\mu = \frac{F_F}{F_N} \tag{1}$$

There are a number of phases from which the values of frictional coefficient can be calculated during the test [29]. The use of different averaging methods has been employed to obtain realistic representative values that best describe sinusoidal plots [30]. This study used the root mean square (RMS) method because it served as a common evaluation parameter relative to frictional coefficient and gave the best

description of the entire process [29]. The RMS is a statistical measure of the amplitude of a varying quantity which is especially useful when the values alternate between positive and negative. Given a set of n values {x1, x2, x3, …., xn}, the root mean square can be calculated using the following formula:

$$x_{rms} = \sqrt{\frac{1}{n}\sum_{i=0}^{n} x_i^2} \tag{2}$$

In analyzing the data, groups of cycles were represented by the RMS frictional coefficient thereby reducing the complex data pattern to a simpler numerical representative value. In order to process the data and generate textual and graphical representations of the results, computer programs written in Microsoft C# 4.0, Matlab and MySQL were used.

2.6.4 Wear Measurements

The wear mass was evaluated gravimetrically and the mass loss obtained from the difference of the final and initial masses was used taking into account the lubricant uptake. The wear behavior was then characterized using the parameter, wear factor, W_F (mm^3/Nm), which was calculated as follows:

$$V_L = \frac{m}{\rho} \tag{3}$$

$$W_F = \frac{V_L}{Fd} \tag{4}$$

where V_L is the volume loss in mm^3, m is the mass loss is in kg, ρ is the density in kg/m^3, F is the applied load in N and d is the sliding distance in m.

2.7 Surface Characterization

A microstructural analysis was done on a Nova NanoSem 230 scanning electron microscope (SEM), (FEI, Holland, Netherlands) to analyze the surface morphology of the specimens after testing. The specimens were coated with carbon for this observation. Also, control specimens were evaluated.

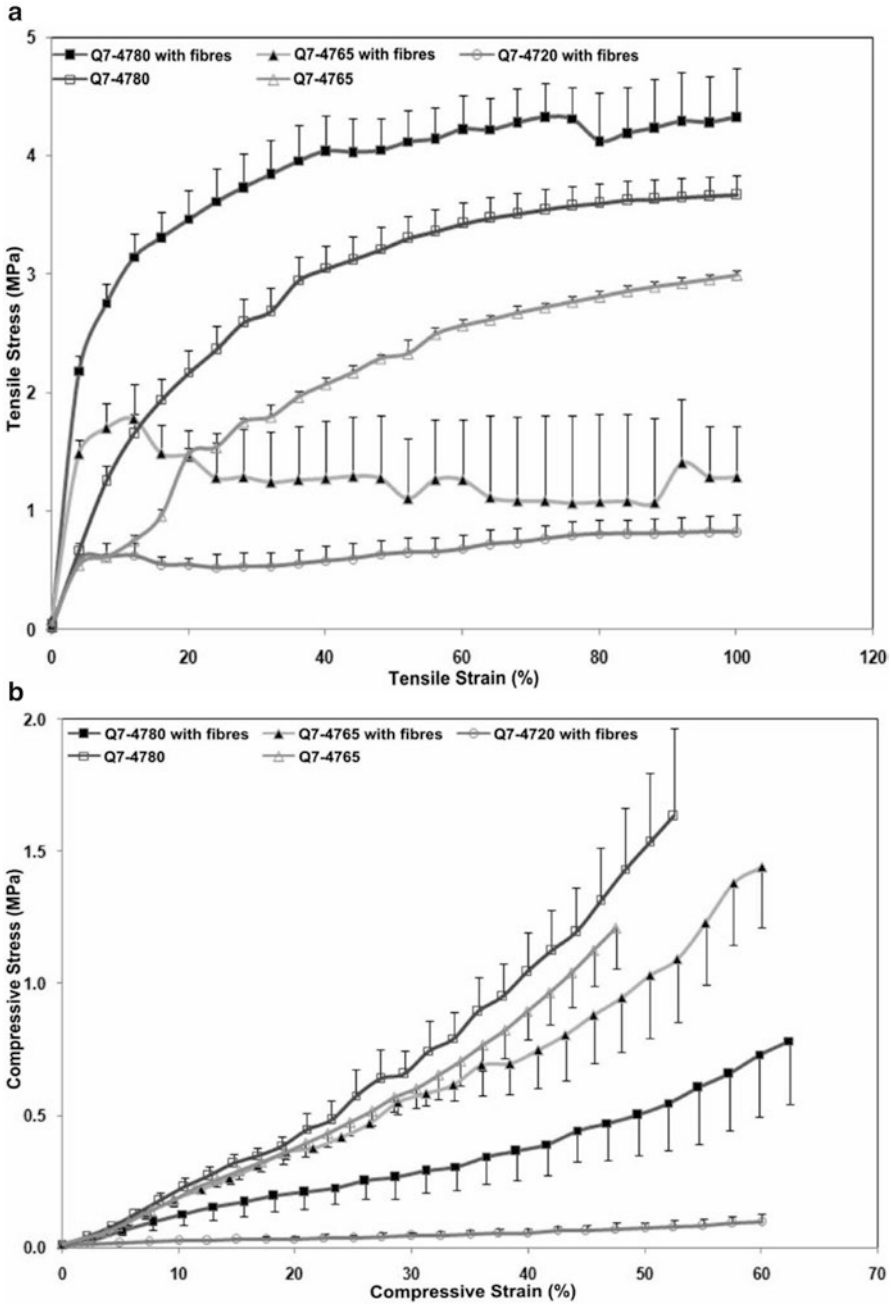

Fig. 8 Tensile (**a**) and compression (**b**) stress–strain plots for the different silicones and their nylon reinforced composites

3 Results and Discussion

3.1 Tensile and Compression Tests

The stress-strain plots for both tension and compression tests for the silicones and their nylon reinforced composites are shown in Fig. 8.

The composite with the optimum properties has its tensile modulus increased significantly from 10.7 ± 2.9 to 114.6 ± 20.9 MPa when reinforced with 5% v/v nylon fibers. This value is within the circumferential tensile modulus of the native meniscus. Unlike the tensile modulus, the compressive modulus of the composite was found to reduce from 2.5 ± 0.6 to 0.7 ± 0.3 MPa when fibers were incorporated; which is closer to the aggregate compressive modulus of the native meniscus. The optimum tensile modulus was observed with composites of silicone elastomer Q7-4780 which increased from 10.7 ± 2.9 MPa for 100% polymeric matrix samples to 114.6 ± 20.9 MPa for composites with reinforced fibers. Its compressive modulus on the other hand reduced from 2.5 ± 0.6 to 0.74 ± 0.3 MPa for samples without fibers and with fibers, respectively.

In the nylon reinforced composites, an increase in the tensile modulus was observed as compared to their unreinforced analogue, and this follows a similar trend as described by a previous research group [16]. In comparison with the composite of Q7-4780 which had the highest tensile modulus, Q7-4765 had a lower modulus of approximately 43% while that of Q7-4720 was the least at approximately 15%.

The lowest compressive modulus value was measured for the composite of Q7-4780 which decreased from 2.5 ± 0.6 to 0.7 ± 0.3 MPa when fibers were incorporated. Although this value is higher than the aggregate compressive modulus of the native meniscus, which is 0.22 MPa [31], this reduction suggests that nylon reinforced silicones can be fashioned to mimic the desired properties of the native meniscus.

In this study, both B8 and B9 displayed characteristic elastomeric stress-strain behavior that is typical of these materials and have also been observed in previous studies for similar PCU materials [32]. The tensile stress-strain curve of B9 showed a slightly higher yield point before undergoing a period of further elongation. The unreinforced PCU materials permitted more strain prior to failure than their fiber-reinforced counterparts (Fig. 9).

The empirically determined tensile modulus of composite of PCU is summarized in Table 3. Conversely, the value of ~18 MPa obtained for the tensile modulus of B9 in the current tests, was lower than 29 MPa given by the supplier.

From the mechanical tests for the different composites, the PCU composites provided excellent mechanical properties more suitable for the meniscus than the silicone composites. Therefore, further tests including friction and wear were conducted on the PCU composite samples.

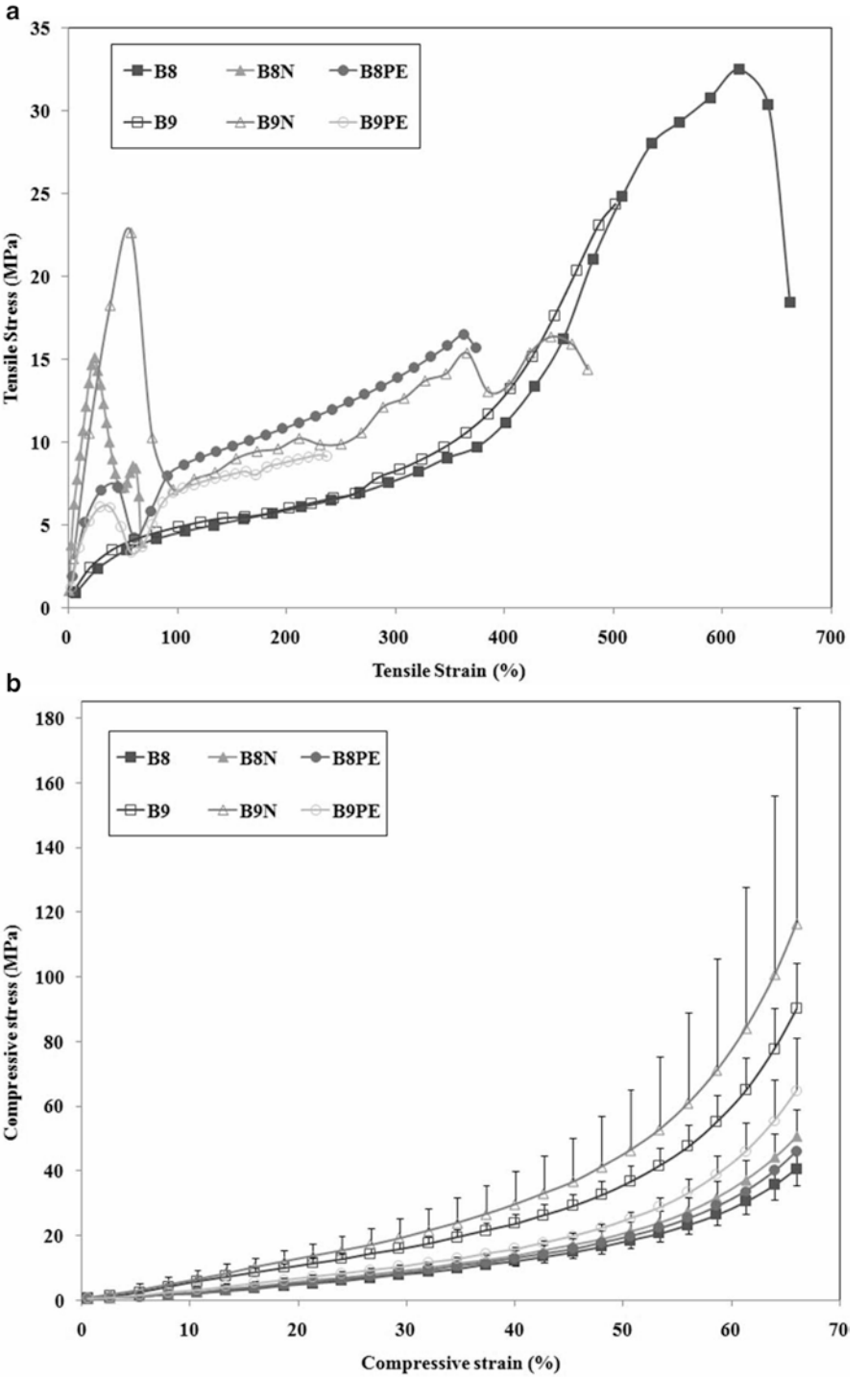

Fig. 9 Tensile and compression stress–strain plots for the different PCU and their nylon and PE reinforced composites

Table 3 Mechanical properties of the fiber-reinforced PCU composites compared with their unreinforced matrices

Specimen type	Tensile modulus (MPa)	Compressive modulus (MPa)
B8	14.12 ± 1.56	18.85 ± 2.07
B8N	64.82 ± 2.10	23.55 ± 1.74
B8PE	46.23 ± 0.03	19.53 ± 1.60
B9	17.63 ± 0.53	71.22 ± 1.03
B9N	123.97 ± 1.67	73.39 ± 6.59
B9PE	43.77 ± 5.07	31.93 ± 0.69

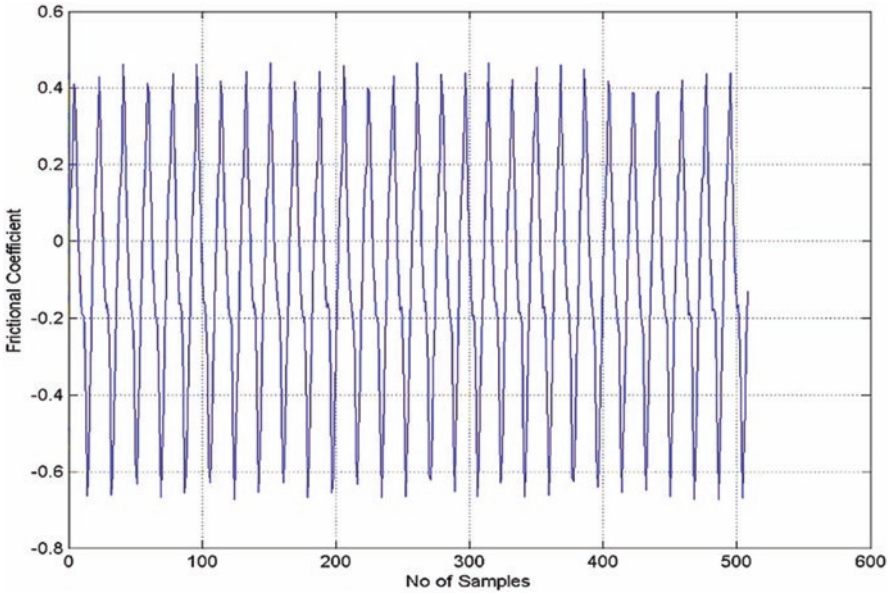

Fig. 10 An excerpt of 20 cycles from the data collected from one of the specimens

3.2 Friction Test for the Produced Meniscal Prosthesis

An output coefficient of friction data taken across 20 cycles is shown in Fig. 10. Considering the plots for the total period for each test performed, it was evident that there were varying (uneven) peaks which appeared almost periodically on each plot. These peaks are background "noise" which could be attributed to the instrumentation set up.

Using the averaging method of effective value (rms) to generate the coefficient of friction, μ_{rms} and the frictional force, distinct, more explicit plots were generated (Fig. 11a, b) which are more representative of the frictional characteristic of the specimens tested.

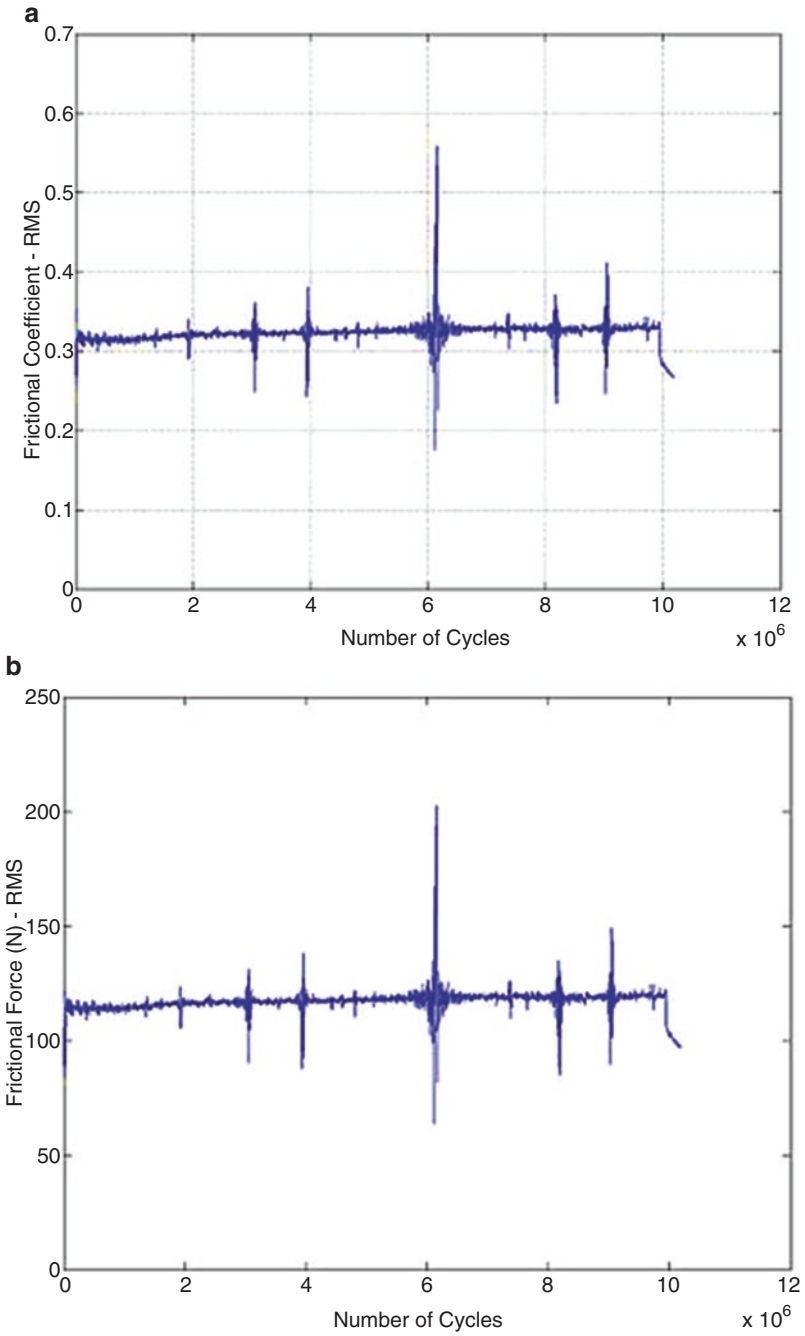

Fig. 11 A representative of the (**a**) coefficient of friction and (**b**) frictional force from the same specimen in Fig. 10 based on rms calculations

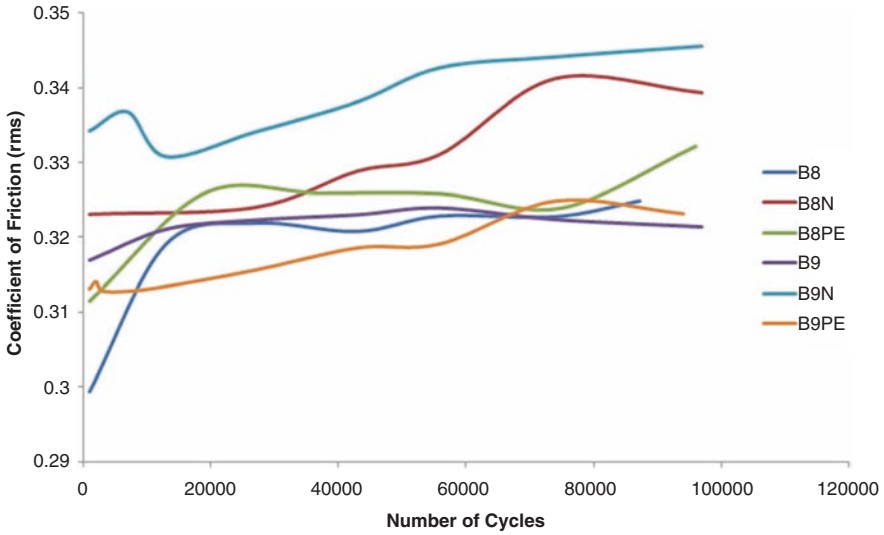

Fig. 12 Mathematical representation of the COF curve as a function of number of cycles

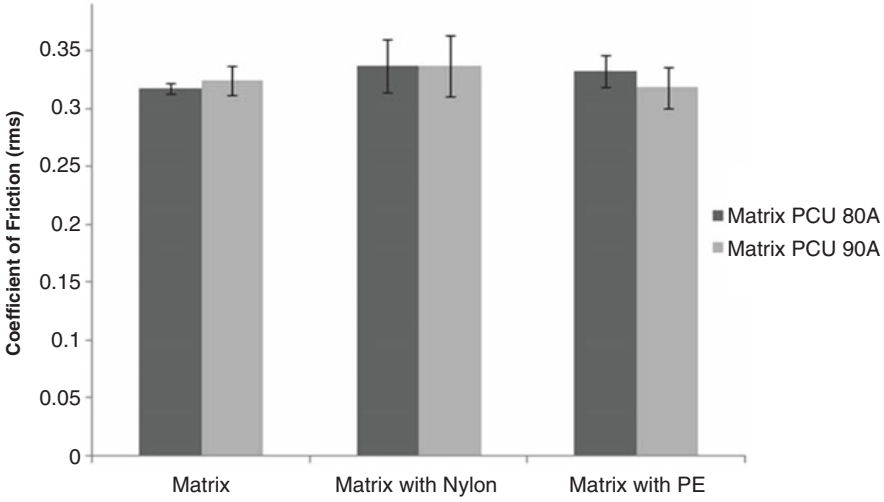

Fig. 13 Comparison of the coefficient of friction in the matrix and fiber-reinforced composite specimens

A plot of the six different compositions tested showed differences in their frictional behavior with respect to time (Fig. 12). In order to compare the behavior of the different tested specimens, the coefficient of friction, μ_{rms} curves were refined by fitting a mathematical function to obtain an average trendline for the experimental data (Fig. 12).

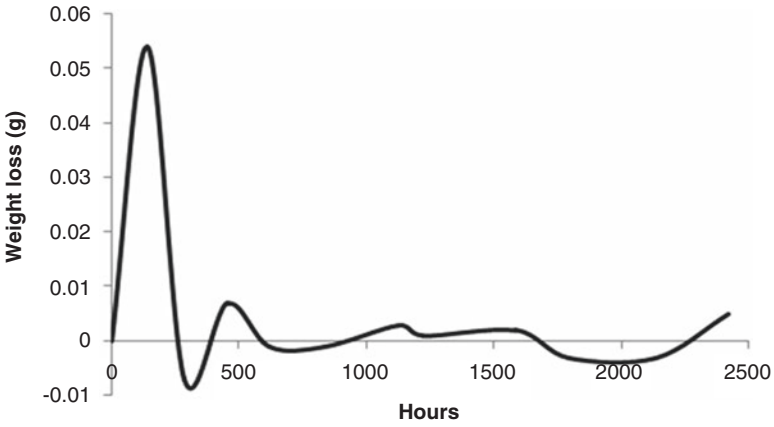

Fig. 14 Vacuum oven test of a representative sample

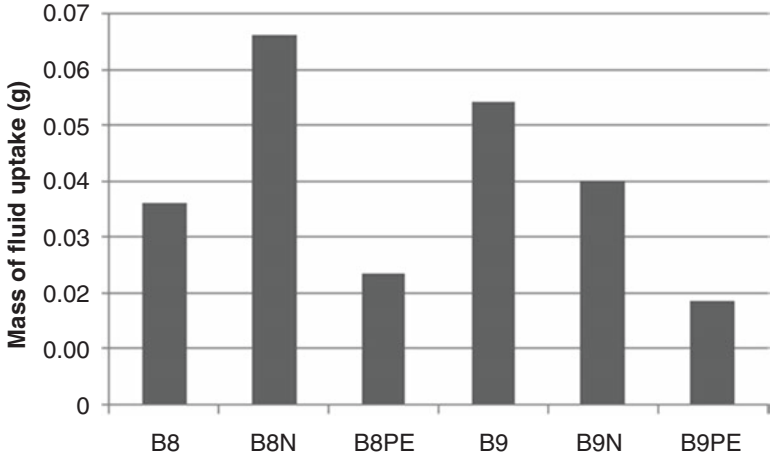

Fig. 15 Fluid uptake observed in the loaded soak controls for the different specimen types

In general, the curves showed an initial increase at the onset of the experiment within the first 20,000 cycles. This was afterwards followed by a phase of fairly constant friction coefficient values. Subsequently, at some point, spiky shifts to higher coefficient of frictions were observed, which was generally followed by a drop in the coefficient of friction.

The effect of fiber reinforcement as well as the fiber types on the friction coefficient was observed in all the specimens tested. The different compositions were observed to vary with respect to the reinforcement fibers (Fig. 13). The friction coefficient for B8 was lower compared to B9 (~2% decrease) while the friction coefficient for both B8N and B9N showed a rise in value (~6% and ~4% respectively) when compared to their respective unreinforced matrices. Although B9PE

Table 4 Calculated wear mass and wear factors for the different specimen types

Specimen prosthesis	Wear mass (mg)	Wear factor × 10^{-6} (mm^3/Nm)
B8	35.0 (±16.0)	10.0 (±6.4)
B8N	47.0 (±18.0)	22.5 (±2.9)
B8PE	4.0 (±2.8)	1.6 (±1.1)
B9	30.0 (±8.0)	10.7 (±3.4)
B9N	20.0 (±1.0)	7.3 (±0.5)
B9PE	6.0 (±4.9)	2.1 (±1.9)

gave a lower friction coefficient than its matrix, the contrary was the case with B8PE. A percentage decrease of ~2% was recorded in the case of B9PE while an increment of ~4% was recorded for B8PE. There was no significant difference observed in the mean value of the friction coefficient between the matrix and their reinforced matrices, and between B8 and B9 as $P > 0.05$.

3.3 Wear Test of the Produced Meniscus

It was observed that vacuum oven drying of the specimens was not effective because it was difficult to obtain a stable weight loss in the specimens even after 100 days of drying (Fig. 14). Similarly, such behavior has been reported by previous studies on PCUs [33, 34]. Hence, these results were not used in the mass loss calculation.

There was marginal difference between the loaded soak and unloaded soak controls in the order of 0.004. However, it was interesting that the fluid absorption varied widely between the different loaded soak controls owing to the differences in the constituent materials (Fig. 15).

It was observed that nylon reinforced PCUs fluid intake was quite high with B8N absorbing the highest amount. The mass loss due to wear varied within the different specimens with B8PE recording the least value and the highest was B8N. Nylon reinforcement fibers were clearly seen to predispose the matrices to excessive mass loss and consequently a high wear factor (Table 4).

A physical examination of the stainless steel counterface showed no presence of the matrix PCU material on its surface at the end of the test. Also, on visual assessment of the prostheses specimens no mark was noticeable on the articulated surface. Micrographs of the tested specimens showed that changes have taken place on the surfaces of specimens as a consequence of wear processes (Fig. 16).

The surfaces of the PCU and the fiber-reinforced specimens showed a rather smooth surface (Fig. 16a, b) while the reinforced specimen appeared even smoother unlike the tested specimens that exhibited surfaces such as bumpy (Fig. 16c, d), striated (Fig. 16c, f and g), rough surface (Fig. 16f) and wear debris (Fig. 16d–g). The wear morphological attributes of the nylon composites, B8N and B9N, revealed more wear debris and deformation, than their respective matrix, B8 and B9. The surfaces were also marked or striated with some continuous lines. Damaged areas

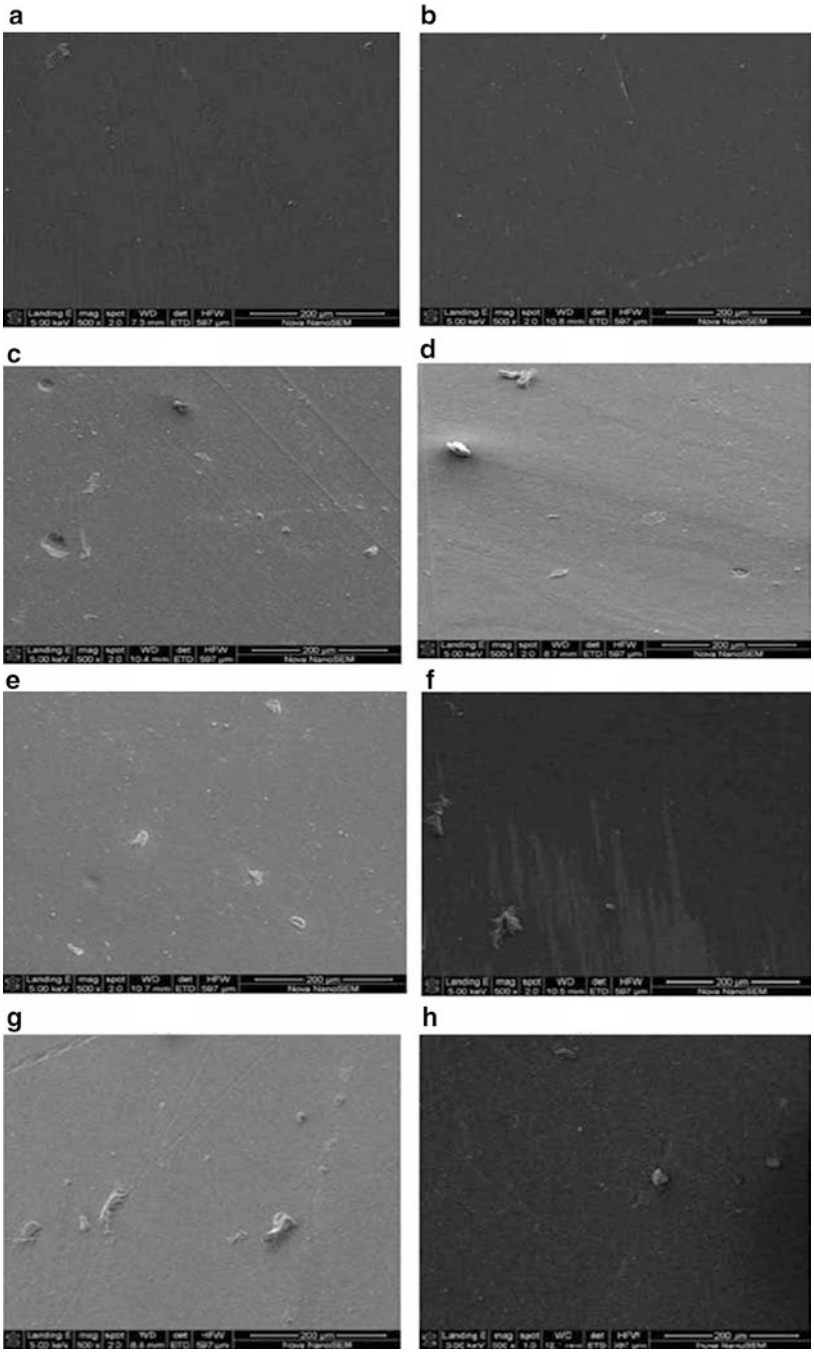

Fig. 16 SEM surface morphology of the specimen types as observed under the SEM. Untested specimen of (**a**) matrix (**b**) reinforced matrix and tested specimens of (**c**) B8 (**d**) B8N (**e**) B8PE (**f**) B9 (**g**) B9N (**h**) B9PE

found on B9 were more than that of B8 consisting of worn scar with minimal wear debris (Fig. 16f).

The wear features apparent with PCU-nylon composites could be due to the influence of nylon fibers having a tendency to hydrolyse when it absorbs fluid thereby losing its stiffness over time and subsequently exhibiting a reduction in wear resistance (Table 4).

The composites containing PCU-PE indicated lower wear debris and lighter deformation with B8PE having a smoother surface other than B9PE. B9PE seemed rougher with delaminated areas which could be connected to fiber pull-out. These composites appeared to have better wear resistance owing to the reinforcement fibers performing the role of a strengthener in the PCU matrix.

The excellent wear properties of PE reinforcements are assumed to withstand the wear processes at the fiber-matrix interface, thereby generating resistance which prevents the removal of the PCU matrix [35].

4 Conclusion

Reinforcing of the PCU matrix with fibers should result in improved friction and wear properties by minimizing plastic deformation and subsequently a reduction in friction and wear rate. However, as seen from this study the type of reinforcement fiber used and its tribological behavior play a role in the overall composite properties. The PE fibers of the type used have favorably affected both the frictional and wear characteristics of the PCU matrix. Both Bionate PCU matrices used have performed satisfactorily for the proposed use considering their behavior especially in the reinforced state. It is proposed that further testing at physiological loading at millions of cycles can be carried out in order to decide on the choice of the matrix for the PE fibers.

The limitations associated with this work include inability to use the friction/wear testing equipment to carry out the experiment at physiological loads experienced in the knee joint. Also, an ideal set up will be to simulate the test using a counterface of bone or cartilage, such that an in vivo system is replicated.

References

1. McDermott ID, Amis AA. The consequences of meniscectomy. J Bone Joint Surg Br. 2006;88:1549–56.
2. Vrancken ACT, Buma P, van Tienen TG. Synthetic meniscus replacement: a review. Int Orthop. 2013;37(2):291–9.
3. Ahmed AM. The load bearing role of the knee mensici. In: Mow VC, Arnoczky SP, Jackson DW, editors. Knee meniscus: basic and clinical foundations. New York: Raven press; 1992. p. 59–73.

4. Aufderheide AC, Athanasiou KA. Mechanical stimulation toward tissue engineering of the knee meniscus. Ann Biomed Eng. 2004;32:1161–74.
5. Pangborn CA, Athanasiou KA. Knee meniscus, biomechanics of Wiley encyclopaedia of biomechanical engineering. New York: Wiley; 2006.
6. Fan RSP, Ryu RKN. Meniscal lesions: diagnosis and treatment. Medsc Orthop Sports Med. 2000;4(2).
7. Vedi V, Williams A, Tennant SJ, et al. Meniscal movement. An in-vivo study using dynamic MRI. J Bone Joint Surg Br. 1999;81(1):37–41.
8. Stone KR. Meniscus replacement. Clin Sports Med. 1996;15(3):557–71.
9. Turner S. General principles and perspectives. In: Hodgkinson JM, editor. Mechanical testing of advanced fibre composites. Boca Raton, FL: CRC; 2000. p. 4–35.
10. Shriram D, Kumar GP, Cui F et al. Evaluating the effects of material properties of artificial meniscal implant in the human knee joint using finite element analysis. Sci Rep. 2017;7.
11. Messner K. Meniscal substitution with a Teflon-periosteal composite graft: a rabbit experiment. Biomaterials. 1994;15(3):223–30.
12. Messner K, Lohmander LS, Gillquist J. Cartilage mechanics and morphology, synovitis and proteoglycan fragments in rabbit joint fluid after prosthetic meniscal substitution. Biomaterials. 1993;14(3):163–8.
13. Sommerlath K, Gallino M, Gillquist J. Biomechanical characteristics of different artificial substitutes for rabbit medial meniscus and effect of prosthesis size on knee cartilage. Clin Biomech (Bristol, Avon). 1992;7:97–103.
14. Klompmaker J, Jansen HW, Veth RP, et al. Porous implants for knee joint meniscus reconstruction: a preliminary study on the role of pore sizes in ingrowth and differentiation of fibrocartilage. Clin Mater. 1993;14(1):1–11.
15. Tienen TG, Heijkants RG, de Groot JH, et al. Meniscal replacement in dogs. Tissue regeneration in two different materials with similar properties. J Biomed Mater Res B Appl Biomater. 2006;76(2):389–96.
16. Holloway JL, Lowman AM, Palmese GR. Mechanical evaluation of poly(vinyl alcohol)-based fibrous composites as biomaterials for meniscal tissue replacement. Acta Biomater. 2010;6(12):4716–24.
17. Elsner JJ, Portnoy S, Zur G, et al. Design of a free-floating polycarbonate-urethane meniscal implant using finite element modeling and experimental validation. J Biomech Eng. 2010;132(9):095001.
18. Kon E, Filardo G, Tschon M, et al. Tissue engineering for total meniscal substitution: animal study in sheep model-results at 12 months. Tissue Eng Part A. 2012;18(15–16):1573–82.
19. Kelly BT, Potter HG, Deng XH, et al. Meniscal allograft transplantation in the sheep knee: evaluation of chondroprotective effects. Am J Sports Med. 2006;34(9):1464–77.
20. Linder-Ganz E, Elsner JJ, Danino A, et al. A novel quantitative approach for evaluating contact mechanics of meniscal replacements. J Biomech Eng. 2010;132(2):024501.
21. Zur G, Linder-Ganz E, Elsner JJ, et al. Chondroprotective effects of a polycarbonate-urethane meniscal implant: histopathological results in a sheep model. Knee Surg Sports Traumatol Arthrosc. 2010;19(2):255–63.
22. Bryce DM. Plastic injection molding: manufacturing process fundamentals. Society of Manufacturing Engineers; 1996. p. 174.
23. Geary C, Birkinshaw C, Jones E. Characterisation of Bionate polycarbonate polyurethanes for orthopaedic applications. J Mater Sci Mater Med. 2008;19:3355–63.
24. Hohl MW. The wear behaviour of UHMWPE and ion implanted UHMWPE against different counterfaces. MSc Thesis, University of Cape Town. 1998.
25. Marcus K. Micromechanisms of polymer sliding wear. PhD Thesis, University of Cape Town. 1992.
26. Klaas NV, Marcus K, Kellock C. The tribological behaviour of glass filled polytetrafluoroethylene. Tribol Int. 2005;38:824–33.

27. Katta JK, Marcolongo M, Lowman A, et al. Friction and wear behaviour of poly(vinyl alcohol)/poly(vinyl pyrrolidone) hydrogels for articular cartilage replacement. J Biomed Mater Res A. 2007;83(2):471–9.
28. Covert RJ, Ott RD, DN K. Friction characteristics of a potential articular cartilage biomaterial. Wear. 2003;255:1064–106.
29. Živić F, Babić M, Mitrović A, et al. Interpretation of the friction coefficient during reciprocating sliding of Ti6Al4V alloy against Al_2O_3. Tribol Ind. 2011;33(1):36–42.
30. Nechak L, Berger S, Aubry E. A polynomial chaos approach to the robust analysis of the dynamic behaviour of friction systems. Eur J Mech A Solids. 2011;30(4):594–607.
31. Scholes SC, Unsworth A, Jones E. Polyurethane unicondylar knee prostheses: simulator wear tests and lubrication studies. Phys Med Biol. 2007;52:197–212.
32. St John K, Gupta M. Evaluation of the wear performance of a polycarbonate-urethane acetabular component in a hip joint simulator and comparison with UHMWPE and cross-linked UHMWPE. J Biomater Appl. 2012;27(1):55–65.
33. Wang J, Gu M. Wear properties and mechanisms of nylon and carbon-fiber-reinforced nylon in dry and wet conditions. J Appl Polym Sci. 2004;93:789–95.
34. Alejandro AJ, Athanasiou KA. Design characteristics for the tissue engineering of cartilaginous tissues. Ann Biomed Eng. 2004;32(1):2–17.
35. De Nardo L, Farè S, Di Matteo V, Cipolla E, Saino E, Visai L, Speziale P, Tanzi MC. New heparinizable modified poly(carbonate urethane) surfaces diminishing bacterial colonization. J Mater Sci Mater Med. 2007;18(11):2109–15.